Unveiling the structural insights of PFAS-β-lactoglobulin binding mechanism mediating neuronal toxicity in neonates.

Shalja Verma[1], Anika Singh[2], Lela Vukovic[3], Mahesh Narayan[3*], Pravindra Kumar[1*]

[1]Department of Biosciences and Bioengineering, Institute of Engineering and Technology, Roorkee, Uttarakhand, 247667, India

[2]Battlefield High School, Haymarket, Virginia, 20169, USA

[3]Department of Chemistry and Biochemistry, The University of Texas at El Paso, El Paso, TX 79968, USA

[*]Corresponding Authors. E-mail: pravindra.kumar@bt.iitr.ac.in; mnarayan@utep.edu

ORCID: Pravindra Kumar: 0000-0003-2128-7736; Mahesh Narayan: 0000-0002-2194-5228

Abstract

The strong electrostatic interaction in C-F bonds contributes to the forever nature of per- and polyfluoroalkyl (PFAS) substances. The frequent use of PFAS in consumer products results in diverse toxic effects. Previous studies present its ability to cross the blood-brain and placental barriers and its presence in breast milk and infant formula, causing severe neurotoxic effects. β-lactoglobulin, a milk protein, transports hydrophobic and amphiphilic compounds to different organs, including the brain. Biochemical and biophysical studies of β-lactoglobulin-PFAS interaction have been promising. The present study reports the complex crystal structures of β-lactoglobulin with PFOA (Perfluorooctanoic acid) at 2.0 (Å), PFOS (Perfluorooctanesulfonic acid) at 2.5 (Å), and PFDA (Perfluorodecanoic acid) at 2.0 (Å), disclosing the high affinity of the three PFAS compounds for the central calyx of β-lactoglobulin. Significant hydrophobic interactions stabilized the binding of the PFAS hydrophobic tail inside the calyx, while polar interactions with residues Lys60 and Lys69 stabilized the polar head group. Comparative structural analysis revealed the presence of an open conformation of the EF loop containing the Glu89 latch residue in the complex structures compared to the apo-form. Molecular dynamics (MD) simulation analysis revealed high stability of the PFAS binding and attainment of global minima in all complexes. The average binding energy of PFDA in β-lactoglobulin calyx was -25.04 kcal/mol, which was higher than PFOS (-21.47 kcal/mol) and PFOA (-22.89 kcal/mol) due to increased van der Waals interactions of the longer hydrophobic chain of PFDA with β-lactoglobulin. Henceforth, this work presents the structural mechanism of PFAS-β-lactoglobulin binding, disclosing β-lactoglobulin as an effective PFAS transporter mediating neurotoxicity in neonates.

Keywords: β-lactoglobulin, Per- and polyfluoroalkyl (PFAS) substances, Neurotoxicity, X-ray crystallography, MD simulation

Introduction

The bond between carbon and fluorine, C-F, possesses high stability due to the highly electronegative nature of fluorine, which generates a strong electrostatic attraction between the partially negative fluorine and partially positive carbon atom (O'Hagan, 2007; Kraka & Cremer, 2009; Marshall & Schwartz, 1997). Such a strong attraction makes the C-F bond the sturdiest among all the bond types in organic chemistry and is "forever" in nature.

The association of C-F bond-containing per- and polyfluoroalkyl (PFAS) substances with adverse human health outcomes has emerged as a major societal and governmental concern (Key et al., 1997). Exposure to these substances can occur through cookware, ingestion of contaminated drinking water, food, and food packaging. Ingestion can also occur through the use of some PFAS-containing consumer products (lipstick, upholstery, hygiene products, diapers, waterproof clothing, stain-resistant carpets and fabrics, and cleaning products), the inhalation of contaminated dust or airborne particles, or dermal contact with contaminated materials (DeLuca et al., 2022). PFAS exposure is linked to obesity, decreased fertility, developmental anomalies in foetuses, neonates, and children, compromised immunity, and increased risk of prostate, kidney, and testicular cancers (Panieri et al., 2022; Fenton et al., 2020; Boyd et al., 2022; Bharal et al., 2024)

Studies have shown that PFAS can cross the blood-brain barrier and may contribute to neuroinflammation, neurotoxicity, cognitive and locomotory decline, all of which promote the progression of Alzheimer's (AD) and Parkinson's diseases (PD) (Starnes et al., 2022; Roy et al., 2025; Y. Cao & Ng, 2021; Kalyn et al., 2023; Marchese et al., 2024). A recent comprehensive study focused on how they affect gene expression of neuronal-like cells (Running et al., 2024). Exposure to a suite of C-F bond-containing organic moieties resulted in modest but distinct changes in lipids and caused over 700 genes to express differently, including those involved in synaptic growth and neural function. The findings also hint that the neurotoxic effects are structure-dependent, highlighting the chemical complexities involved (C-F chain-length, head-group, and branching) (Running et al., 2024). Elsewhere, a study revealed that multigenerational exposure of the nematode *C. elegans* to PFNA significantly increased mutation frequencies of progeny by preferentially inducing T: A → C: G substitutions and small insertion-deletions within repetitive regions (Z. Cao et al., 2024). Mechanistic analyses suggested that the said PFAS elicited DNA double-strand breaks.

PFAS is observed to accumulate in the kidney, liver, and lung. For example, perfluorobutanoic acid was the most frequently found PFAS (and at the highest concentrations with median values residing at 263 and 807 ng/g in kidney and lung, respectively) (Abraham et al., 2021). In the liver and brain, perfluorohexanoic acid showed the maximum levels (median: 68.3 and 141 ng/g, respectively), while PFOA was the most prevalent PFAS in bone (median: 20.9 ng/g) (Pérez et al., 2013). In the serum of fishery workers, PFAS levels ranged between 0.01 and 10,400 ng/ml, while those exposed to contaminated drinking water presented with levels ranging between 0.5–35.5 ng/ml, suggesting that occupational exposure can result in PFAS burdens 1-4 orders of magnitude

higher than the general population (Zhou et al., 2014). PFAS have been detected in serum from the umbilical cord and newborn blood, demonstrating that these chemicals are capable of passing through the placental barrier with estimates of the efficiency of placental transfer ranging between 30-79% (Mahfouz et al., 2023). Breast milk has been shown to account for 83-99% of PFAS total daily intake for infants (Yao et al., 2023; Nyberg et al., 2018). A study involving 50 lactating mothers revealed 16 PFAS compounds in 4-100% of the samples (Zheng et al., 2021). Therein, PFDA was found in 94% of the cohort, with the median residing at 7.4 pg/ml. Perfluorooctanesulfonic acid (PFOS) and perfluorooctanoic acid (PFOA) were the most abundant PFAS in these samples (medians 30.4 and 13.9 pg/mL, respectively). PFAS presence has also been detected in infant formulas either innately or post-reconstitution (Mokhtari et al., 2024; Martin et al., 2016). The hydrophobic nature of PFAS, coupled with the presence of α-lactalbumin in human milk and both β-lactoglobulin and α-lactalbumin in infant formulas, provides the motivation to examine the impact of PFAS exposure on the structure and function of milk proteins.

β-lactoglobulin is a major protein of ruminant milk that accounts for 10-15 % of its protein content (Narayan & Berliner, 1997; Tai et al., 2016). It contributes to a major fraction of whey protein and acts as a transporter for hydrophobic metabolites and amphiphilic compounds, regulates the activity of pregastic lipase in the neonatal stage, and protects retinol from light-mediated degradation (Perez et al., 1992). From the aforementioned literature, it is highly likely that contaminated milk matrices provide a conduit for the interaction of β-lactoglobulin and PFAS.

Several studies have proposed a high binding affinity of PFAS for β-lactoglobulin using biochemical, biophysical, and in-silico approaches and have discussed the role of β-lactoglobulin in PFAS transport to different organs (Schwieger & Ropers, 2012; Pham et al., 2024; Yadav et al., 2024). However, structural studies revealing the exact binding mechanism of the PFAS in β-lactoglobulin utilizing X-ray crystallography have not been conducted. Such studies can be beneficial for devising the binding and transport mechanism of PFAS by β-lactoglobulin and identifying binding inhibition approaches to reduce milk contaminants.

The present study determined the crystal structures of β-lactoglobulin in complex with PFOA (Perfluorooctanoic acid), PFOS (Perfluorooctanesulfonic acid), and PFDA (Perfluorodecanoic acid), revealing structural intricacies mediating the binding of PFAS in the β-lactoglobulin central calyx. Furthermore, in-depth molecular dynamics simulation

analysis of the crystal structures was performed to analyze the stability and dynamic changes communicated by the binding of PFAS in β-lactoglobulin.

This analysis forms part of our overarching objective to develop a precise understanding of the electrostatic, van der Waals, H-bonding, London Dispersion forces, along with hydrophobic effects, also modulated by the nature of the C-F moieties (chain-length, head-group, branching), that may potentially impact human health by compromising nutritional sufficiency and by seeding pathological outcomes. It can begin to lay the roadmap for mechanisms by which commonly used and environmentally prevalent C-F containing chemistries corrupt protein structures and drive neurotoxic outcomes *in vitro* and *in vivo*.[17-22]

Materials and methods

Co-Crystallization of β-lactoglobulin-PFAS complex

The β-lactoglobulin of bovine milk and the PFAS, including PFDA (Perfluorodecanoic acid), PFOA (Perfluorooctanoic acid), and PFOS (Perfluorooctanesulfonic acid), were procured from Sigma Aldrich. The lyophilized powder of β-lactoglobulin was dissolved in MiliQ water up to a concentration of 80 mg/ml and delipidated using activated charcoal at pH 3. The concentration of the delipidated protein was obtained to be approximately 40 mg/ml (Wu et al., 1999). The protein was incubated with the PFAS compounds for 10 min at 20 °C at a concentration of 10 mM. Crystallization was performed using the sitting drop method at a protein to reservoir ratio of 1:3, and screening of different crystallization conditions was performed using crystallization screens to obtain complex crystals of β-lactoglobulin with PFAS (Dessau & Modis, 2011). The cube-shaped crystals of β-lactoglobulin in complex with PFAS were obtained in a crystallization condition containing 1.8 M sodium phosphate monobasic monohydrate and potassium phosphate dibasic at pH 8.2.

Data Collection and structure solving

The collection of X-ray data was performed using a Rigaku Micromax-007 HF microfocus high-intensity rotating anode X-ray generator installed with a Rigaku Hypix 6000C detector available at home source at the Macromolecular Crystallography Unit, IIC, IIT Roorkee. The diffraction data indexing and integration were performed using CrysAlisPro Software. The data scaling and merging were done using the AIMLESS program of the CCP4i2 v.8.0.019 suite, followed by initial phasing by molecular replacement, considering the apo structure of β-lactoglobulin (PDB ID: 1B0O) as the search model, using the MOLREP program of the CCP4i2 suite [Potterton et al., 2018; Evans & Murshudov, 2013; Vagin & Teplyakov, 2009).

Iterative rounds of model building were performed using the COOT program, and the refinement of the structure at each step was performed using the REFMAC program of the CCP4i2 suite (Emsley et al., 2010; Murshudov et al., 2011). The difference Fourier maps of the PFAS-β-lactoglobulin complexes revealed electron densities of PFAS compounds at levels above 3σ, permitting modelling of PFAS into the density. Omit maps were made using Phenix v.1.18.2-3874 (Adams et al., 2010). The 3D and 2D interaction images were generated using ChimeraX 1.8 and PyMol v.2.5.5 (Pettersen et al., 2020; Rigsby & Parker, 2016).

Molecular Dynamics Simulation

Molecular dynamic simulations of crystal structures of β-lactoglobulin-PFAS complexes and apo β-lactoglobulin were performed using GROMACS 2019.5 software for a 100 ns duration to study the dynamics of interactions between the protein and PFAS (Pronk et al., 2013). The missing residues of flexible regions in crystal structures due to the absence of electron density were added using Coot software. The topologies of PFAS compounds were generated using CGenFF webserver integrated with the CHARMM force field, while the protein topology was generated by applying the CHARMM36 force field using the pdb2gmx tool of GROMACS (Vanommeslaeghe et al., 2009; Huang, & MacKerell, 2013). The apo-protein and complexes were then solvated in a dodecahedron box. The solvated systems were neutralized by sodium ions and then were subjected to energy minimization at a maximum force limit of 10 kJ/mol. Further, number of atoms, volume, temperature (NVT), and number of atoms, pressure, temperature (NPT) equilibrations each for 100 ps were performed. Eventually, each system was subjected to MD production run of 100 ns each. The trajectories of MD simulations were analyzed for Root Mean Square Deviations (RMSD), Root Mean Square Fluctuations (RMSF), Radius of gyration (Rg), Solvent Accessible Surface Area (SASA), B-factor, and secondary structure changes during the simulation (Hollingsworth & Dror, 2018). The PCA analysis of the trajectory frames/conformations was performed, and free energy landscapes were generated for apo as well as PFAS complexes of β-lactoglobulin. The clustering analysis of the simulation trajectories was performed to evaluate the most consistent interactions during the simulation trajectories (Papaleo, et al., 2009). The end state free binding energy analysis for the last 40ns of the simulation trajectories was performed using gmx_mmpbsa v1.6.4 (Valdés-Tresanco et al., 2021). The interaction images of the trajectories were generated using PyMol v.2.5.5, and the plots were prepared using Origin 2024b software (https://www.originlab.com/) (Rigsby & Parker, 2016).

Results and discussion

Crystal of β-lactoglobulin in complex with PFAS compounds

The crystal structures of β-lactoglobulin in complex with PFOS, PFOA, and PFDA were determined in the P 3_2 2 1 space group with one molecule in an asymmetric unit. The statistics of data collection and refinement of three complex structures are presented in Table 1. The 162 amino acid long β-lactoglobulin protein (MW~ 18,400) folds into 8 anti-parallel β-strands forming the β-barrel or the calyx, a characteristic of lipocalin family proteins. The 9th strand, lying near the first strand, is responsible for dimerization, and a 3-turn alpha-helix lies at the outer surface (Figure 1A, B). Two intrachain disulfide bonds, Cys60-Cys160 and Cys106-Cys119, were observed, and the density for the residues Ala111-Glu114 in the GH loop was partial or missing in all three complex structures due to the high flexibility of this loop (Wu et al., 1999). The EF loop, which acts as a gate over the calyx, was observed in open conformation, and the side chain of the latch residue Glu89 was shifted outward of the calyx to enable binding of the PFAS compounds (Pham et al., 2024; Yadav et al., 2024).

Table 1: Refinement statistics of the crystal structures of PFDA-β-lactoglobulin, PFOA-β-lactoglobulin, and PFOS-β-lactoglobulin complexes.

Parameters	**PFDA-β-lactoglobulin complex**	**PFOA-β-lactoglobulin complex**	**PFOS-β-lactoglobulin complex**
Resolution range (Å)	22.49 - 2.0 (2.07 - 2.0)	22.52 - 2.0 (2.07 - 2.0)	23.11 - 2.5 (2.58 - 2.5)
Space group	P 3_2 2 1	P 3_2 2 1	P 3_2 2 1
Unit cell	53.02 53.02 111.15 90 90 120	53.13 53.13 109.98 90 90 120	53.36 53.36 110.19 90 90 120
Total reflections	184566 (13802)	186786 (13707)	126812 (8929)
Unique reflections	12785 (1245)	12696 (1235)	6691 (645)
Multiplicity	14.4 (11.1)	14.7 (11.1)	19.0 (13.8)
Completeness (%)	99.82 (100.00)	99.73 (99.92)	99.70 (99.85)
Mean I/sigma(I)	40.63 (3.85)	53.33 (4.05)	21.94 (1.75)
Wilson B-factor	29.43	29.81	37.24
R-merge	0.07 (0.59)	0.06 (0.51)	0.16 (1.9)
R-meas	0.07 (0.62)	0.06 (0.54)	0.16 (2.03)
R-pim	0.017 (0.18)	0.015 (0.16)	0.037 (0.55)
CC1/2	1 (0.91)	1 (0.93)	1 (0.40)
CC*	1 (0.98)	1 (0.98)	1 (0.76)
Reflections used in refinement	12780 (1247)	12680 (1236)	6685 (646)
Reflections used for R-free	638 (46)	616 (59)	343 (48)

R-work	0.19 (0.27)	0.21 (0.34)	0.23 (0.28)
R-free	0.24 (0.30)	0.25 (0.40)	0.29 (0.39)
CC(work)	0.96 (0.74)	0.93 (0.70)	0.92 (0.56)
CC(free)	0.93 (0.76)	0.92 (0.57)	0.87 (0.54)
Number of non-hydrogen atoms	1408	1406	1324
macromolecules	1332	1322	1280
ligands	50	41	34
solvent	26	43	10
Protein residues	158	159	159
RMS(bonds)	0.011	0.011	0.011
RMS(angles)	2.14	2.2	2.3
Ramachandran favored (%)	96.1	93.55	90.32
Ramachandran allowed (%)	3.9	5.81	5.81
Ramachandran outliers (%)	0	0.65	3.87
Rotamer outliers (%)	7.89	10.14	13.99
Clashscore	24.94	18.46	19.78
Average B-factor	28.47	29.05	26.8
macromolecules	27.25	28.05	26.25
ligands	53.75	43.44	44.83
solvent	42.5	46.05	35.27
Number of TLS groups	1	1	1

- Values in bracket represent last resolution shell values

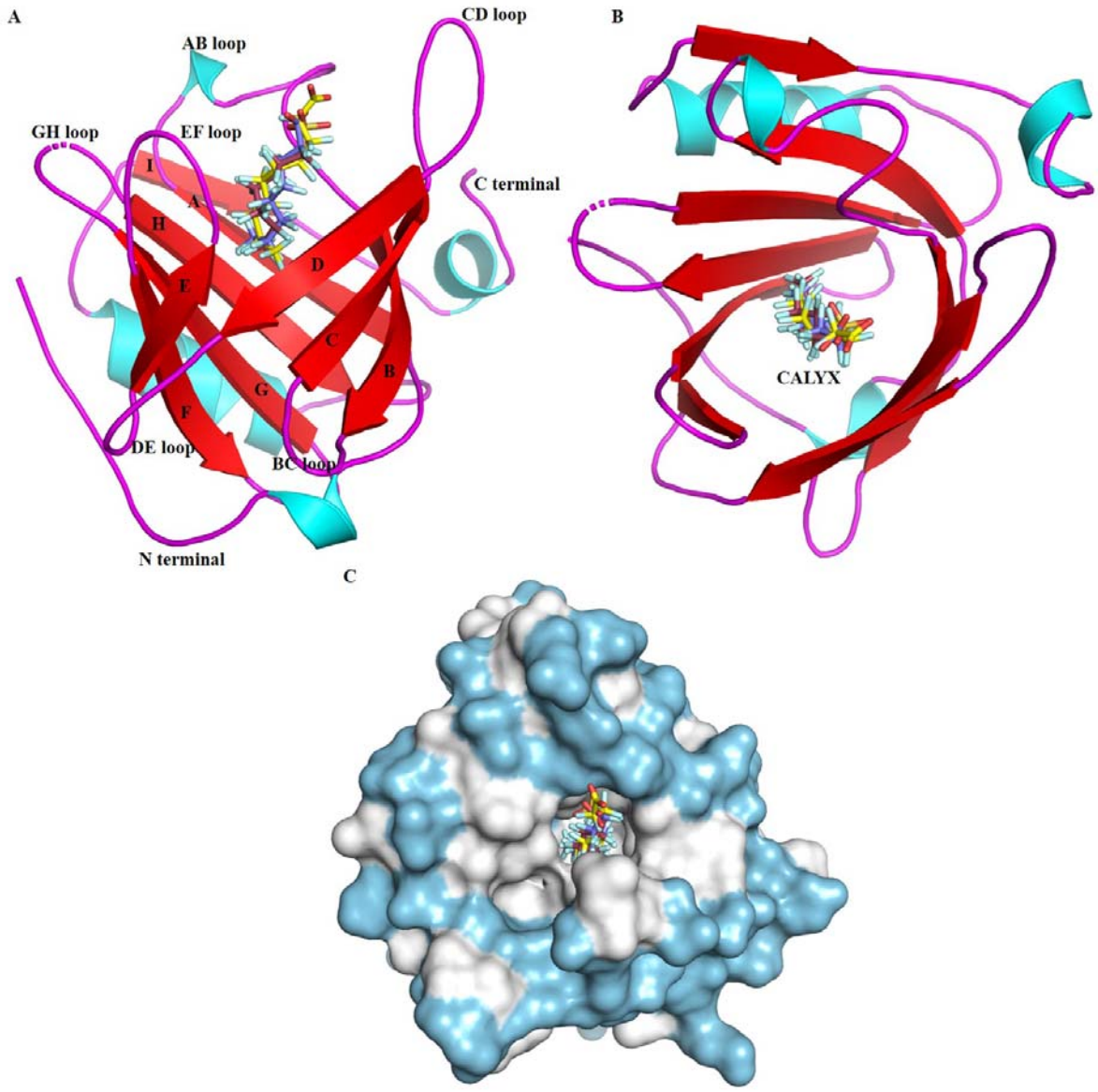

Figure 1: Superimposition of crystal structures of beta-lactoglobulin in complex with PFOS (ruby), PFOA (blue), PFDA (yellow) A). Vertical view showing 9 beta-strands interspersed by loops and helices forming a central calyx with all three compounds bound into it. B) Horizontal view showing the same binding site inside the central calyx for all three compounds. C) Hydrophobic surface view of beta-lactoglobulin showing the presence of highly hydrophobic residues inside the central calyx. (Hydrophobic residue: white, hydrophilic residues: blue)

The difference Fourier maps showing electron densities for the respective PFAS compounds were observed in the central cavity formed by the 8-β-strand calyx in complex structures (Figure 2). The hydrophobic tail of the PFAS compounds extends inside the hydrophobic

cavity, forming hydrophobic interactions with Leu39, Ile56, Leu58, Ile71, Ile84, Val92, Phe105, Met107, and Val41, while the hydrophilic polar head group was stabilized by the hydrogen bond interactions with Lys60 and Lys69 at the cavity entrance (Figure 1C). The placement of the phenyl ring of Phe105 just in front of the terminal CF_3 and subsequent CF_2 groups of the PFAS compounds in all three crystal complex structures hindered the compounds from extending straight deep into the calyx cavity and led to a curved orientation of the compounds. Also, steric repulsion among fluorine atoms along with their large van der Waals radius, in PFAS compounds, causes twisting of the carbon backbone resulting in 15/7 helix conformation, compared to zig-zag conformation of hydrocarbon analog, as observed in the crystal structures (Leung et al., 2023).

The crystal structure of β-lactoglobulin-PFOS complex was solved at 2.5 Å with R_{work} of 0.21 and R_{free} of 0.26. The Gln5, Lys60, and Ser150 residues were present in alternate conformations. The O3 oxygen atom of the sulphonic acid group formed a hydrogen bond with the NZ nitrogen atom of Lys60 at a distance of 2.84 Å. While the O2 oxygen atom of the sulphonic group was at a distance of 3.13 Å from the same nitrogen atom of Lys60. Further, the NZ nitrogen atom of Lys69 was at a hydrogen bond distance of 3.2 Å from the O3 oxygen of the sulphonic acid group of PFOS, revealing potential interactions. Similar interactions of the carboxyl group of palmitates at a distance of 2.72 Å and 3.22 Å with the NZ nitrogen atom of Lys60 and Lys69, respectively, have been observed in previous studies, stabilizing the binding of palmitate in the calyx of β-lactoglobulin (Figure 2A and B) (Wu et al., 1999). In the β-lactoglobulin-PFOA complex at 2 Å with R_{work} and R_{free} of 0.21 and 0.25, Gln5, Ser30, Gln35, Lys47, Lys60, Lys69, Thr125, and Ile162 residues were present in alternate conformations. The O1 oxygen atom of the carboxyl group of the PFOA formed a hydrogen bond with the NZ nitrogen atom of Lys69 at a distance of 3.30 Å. A water molecule lying in close vicinity to the carboxyl group of PFOA in turn formed a hydrogen bond with the O1 oxygen atom of PFOA at a distance of 2.64 Å. The O2 oxygen atom of PFOA formed a hydrogen bond with the NZ nitrogen atom of Lys60 at a distance of 2.92 Å (Figure 2C and D). The complex crystal structure of β-lactoglobulin-PFDA was determined at 2 Å, and R_{free} and R_{work} values were 0.19 and 0.24, respectively, with Val3, Thr18, Asp28, Gln59, Lys60, Ile72, Leu95, Val118, Cys119, Lys135, Met145, and Glu158 in alternate conformations. The PFDA bound to β-lactoglobulin exhibited hydrogen bonding of the NZ nitrogen atom of Lys60 at a distance of 2.49 Å with the O2 oxygen atom of the carboxyl group of PFDA, thus stabilizing the binding of PFDA in the calyx of β-lactoglobulin (Figure 2E and F). Previous

structural studies have reported similar hydrogen bond interactions of Lys60 and Lys69 residues of β-lactoglobulin in stabilizing the binding of long-chain fatty acids having structural homology with PFAS compounds (Wu et al., 1999; Kontopidis et al., 2002).

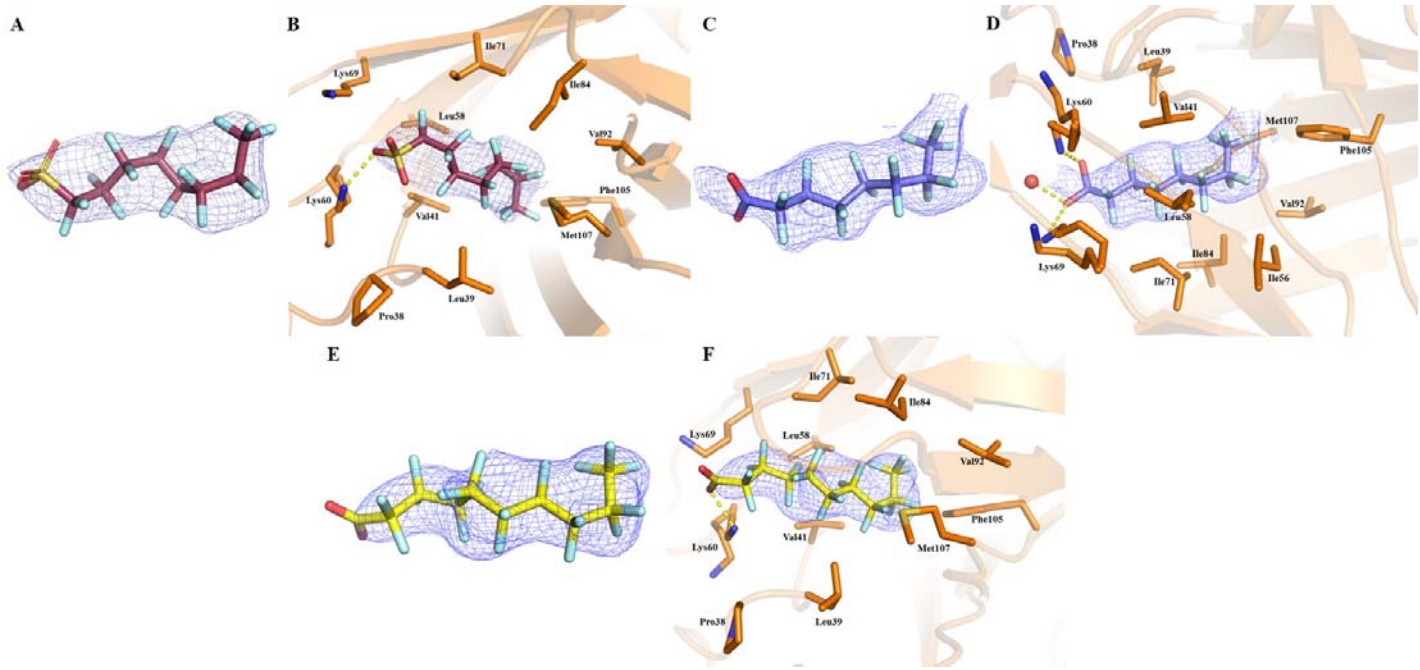

Figure 2: Crystal structures of beta-lactoglobulin with PFASs. A) Electron density Fo-Fc map contoured at 3σ of Perfluorooctane sulfonic acid (PFOS) in complex with beta-lactoglobulin at 2.5 Å B) Stick representation of interacting residues (orange) with PFOS (ruby) in the central calyx of beta-lactoglobulin. C) Electron density F_o-F_c map contoured at 3σ of Perfluorooctanoic acid (PFOA) in complex with beta-lactoglobulin at 2.0Å D) Stick representation of interacting residues (orange) with PFOA (blue) in the central calyx of beta-lactoglobulin E) Electron density Fo-Fc map contoured at 3σ of Perfluorodecanoic acid (PFDA) in complex with beta-lactoglobulin at 2.0 Å F) Stick representation of interacting residues (orange) with PFDA (yellow) in the central calyx of beta-lactoglobulin

Comparison of β-lactoglobulin PFAS complexes open conformation with apo-β-lactoglobulin closed conformation

Structural superimposition of the β-lactoglobulin PFAS complexes crystallized at pH 8.2 over the apo-β-lactoglobulin form crystallized at pH 5.2 (PDB ID: 2AKQ, previous study) revealed an angular displacement of ~ 64.6° in outward direction in the EF loop (at pH 8.2) in all complexes (Adams et al., 2006). This conformational change in the EF loop is mediated

by the variation in pH, where acidic pH leads to closure of the loop while neutral or basic pH results in open conformation of the loop (Figure 3A). The surface representation depicts complete closure of the central cavity by the EF loop and the side chain of Glu89, the latch residue, at acidic pH in the apo-β-lactoglobulin structure, while an open central cavity was visible in the PFAS-β-lactoglobulin complexes reported in this study (Figure 3B, C, D) (Adams et al., 2006). Moreover, significant changes in conformations of the AB and GH loops were also observed. The residues Asp28 to Asp33 in the AB loop formed a small 3_{10} helix in the apo-β-lactoglobulin, while in β-lactoglobulin PFAS complexes, these residues were present in loop conformation. Further, Glu112 to Ser116 of the GH loop were in helical conformation in the apo-form, while in β-lactoglobulin PFAS complexes, residues Ala111-Glu114 were missing and no helical conformation was observed in this loop; thus, PFAS binding mediates alpha-helicity reduction in β-lactoglobulin (Figure 3A) (Wu et al., 1999; Kontopidis et al., 2002; Adams et al., 2006). All these structural changes in β-lactoglobulin in the presence of PFAS compounds illustrate the PFAS binding mechanism of the β-lactoglobulin, revealing its ability to transport PFAS concentration in human milk from maternal serum, eventually increasing the PFAS concentration in neonates.

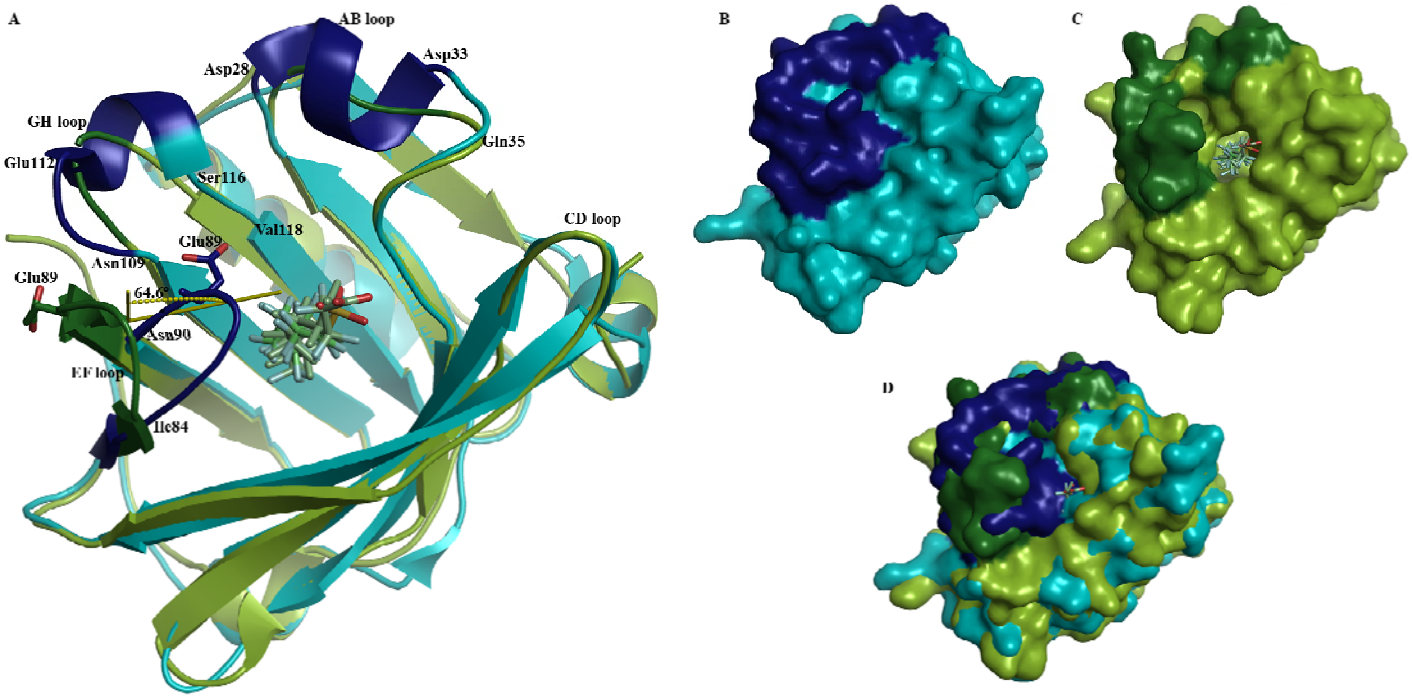

Figure 3: Comparative structural analysis of closed and open conformations of the β-lactoglobulin-PFAS complexes. A) Cartoon representation of superimposed structures of apo-β-lactoglobulin closed (blue) conformation (PDB ID: 2AKQ, previous study) over open

conformation (green) of β-lactoglobulin-PFAS complexes (present study), representing structural changes highlighted in dark green colour for open conformation and dark blue colour for closed conformation. B) Surface view of the apo-β-lactoglobulin closed (blue) conformation (PDB ID: 2AKQ, previous study) C) Surface view of open conformation (green) of β-lactoglobulin-PFAS complexes D) Superimposed surface view of closed (blue) and open (green) conformations of β-lactoglobulin.

Molecular dynamics simulation analysis

Molecular dynamics simulation of crystal structures of β-lactoglobulin-PFDA, β-lactoglobulin-PFOS, β-lactoglobulin-PFOA complexes, and apo-β-lactoglobulin was performed for a duration of 100 ns each to study the PFAS binding dynamics of β-lactoglobulin. The MD simulation trajectory analysis revealed consistent binding of the PFAS molecule in the central calyx cavity of the β-lactoglobulin. The RMSD versus trajectory time plots showed convergence of all the trajectories after 20 ns within a narrow range of ~ 0.20 to 0.30 nm with comparatively higher variations in the β-lactoglobulin-PFOS complex attributed to the presence of the sulphonic acid moiety (Figure 4A) (Hollingsworth & Dror, 2018). The Rg versus time plots revealed consistent compactness of protein in all complexes within the range of 1.50 to 1.55 nm. The higher Rg values of the β-lactoglobulin-PFOS complex corresponding to the RMSD variations were observed, indicating significant conformational changes in the protein structure, conveying a minor reduction in the compactness of the protein (Figure 4B) (Ormeño & General, 2024). The RMSF versus residue plots showed significant fluctuations in the residues ranging from 80-85 and 110-120 in all three complexes, which correspond to the opening of the EF loop and GH loop, respectively. Specific fluctuations in residues 30-40, 127-133, and 150-160 were observed in β-lactoglobulin-PFOA, PFDA, and PFOS complexes, respectively (Figure 4C). Similar variations in the B-factor versus residue plots were observed, indicating increased flexibility of the residues. The 30-40 residue region, which displayed a high B-factor in β-lactoglobulin-PFOA complex, indicates comparatively high flexibility of the AB loop in this complex. The 127-133 residue regions corresponding to the loop between the 8th strand and the 3-trun alpha-helix lying at the base of the calyx showed high flexibility in the B-factor plot and thus high fluctuations in this region of the β-lactoglobulin-PFDA complex. Such fluctuations at the base of the calyx were due to the insertion of the longer chain of PFDA into the central cavity of the calyx, which conveyed conformational changes. Further, the 152-158 residue region of the β-lactoglobulin-PFOS complex indicates the C-terminal small helix suffered

effective fluctuations during the trajectory (Figure 4D and 5) (Pham et al.,2024). The solvent accessible surface area versus time plots shows relative increase in the surface area of the β-lactoglobulin-PFOS complex compared to the other two complex structures of PFOA and PFDA with β-lactoglobulin though the overall change in surface area fluctuated in the fine range of 92 to 107 nm^2 in all the three complex structures indicating stable binding of PFAS compounds in the central cavity along with considerable changes in the protein structure without communicating any misfolding or unfolding (Figure 4E) (Badar et al., 2022). The hydrogen bond versus trajectory time plots revealed significant hydrogen bonding of PFAS compounds with the β-lactoglobulin. Trajectory analysis revealed the consistent hydrogen bond interactions of PFAS compounds with Lys60 and/or Lys69 during the simulation trajectory (Figure 4F).

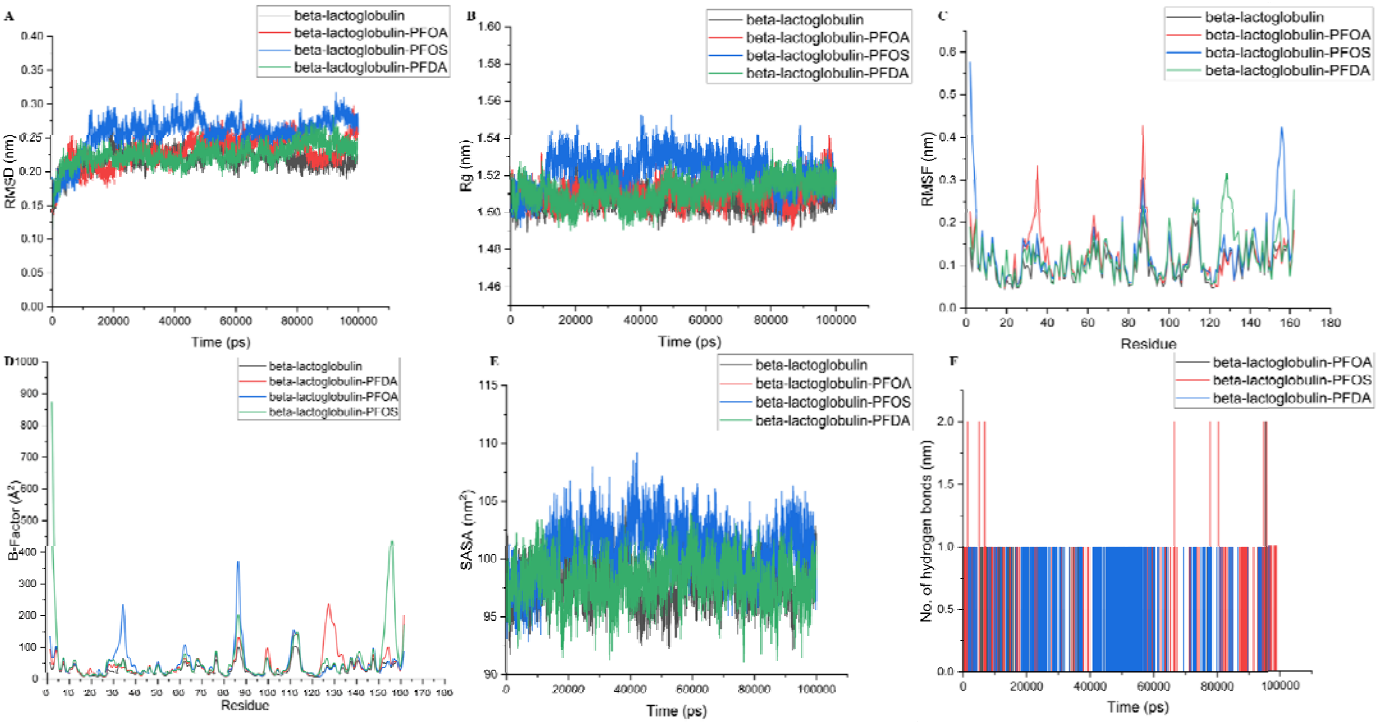

Figure 4: MD simulation analysis of apo-beta-lactoglobulin and crystal structures of beta-lactoglobulin in complex with PFOA, PFOS, and PFDA. A) Root Mean Square Deviation (RMSD) versus time plots B) Radius of gyration (Rg) versus time plots C) Root Mean Square Fluctuations (RMSF) versus residue plots D) B-Factor versus residue plots during 100 ns of simulation trajectory E) Solvent Accessible Surface Area (SASA) versus time plots F) Number of Hydrogen bonds versus time plots.

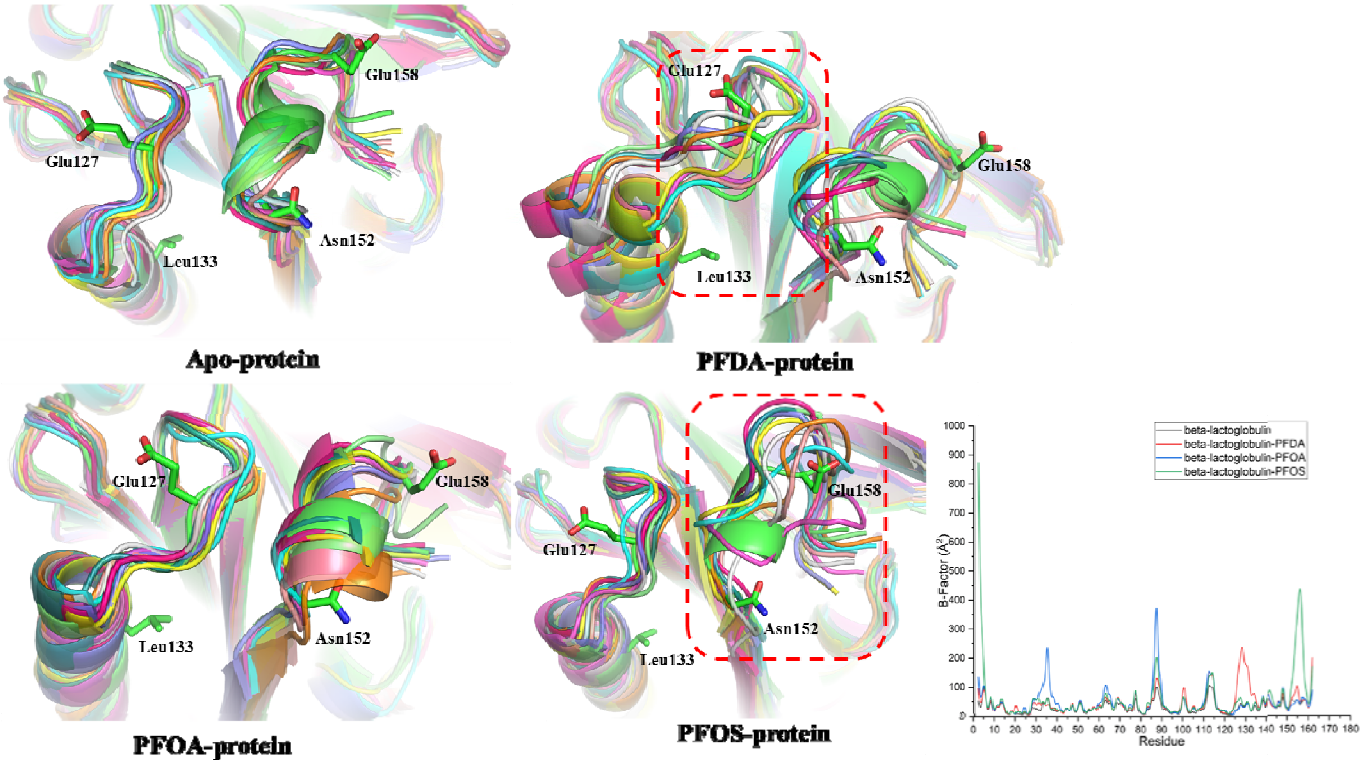

Figure 5: Superimposition of extracted frames at every 10 ns of the MD simulation trajectories of apo-beta-lactoglobulin and crystal structures of beta-lactoglobulin in complex with PFOA, PFOS, and PFDA. The region showing major changes in the B-factor has been marked. Structures in green colour show the initial conformations at 0 ns

The secondary structure analysis elucidated significant variations in the coil, bend, and helical conformations in complex forms compared to the apo-β-lactoglobulin. The major reduction in 3-helix content was observed in the β-lactoglobulin-PFDA complex during the simulation trajectory (Figure 6) (Yadav et al., 2024). The cluster analysis revealed a significant number of structural conformations in the top 10 clusters of all three complexes. The representative conformations of the top 10 clusters depicted consistent binding of the PFAS compounds in the central calyx of the β-lactoglobulin during the trajectory. An open extended conformations of the EF and GH loops were observed in all the complex clusters, while the AB loop was shifted inside the cavity. Significant changes in the cavity volume were evident in β-lactoglobulin-PFAS complexes during the trajectory. The volume of the cavity varied in the range of 616.38 $Å^3$ to 1064.62 $Å^3$ in β-lactoglobulin-PFDA complex, 497.50 $Å^3$ to 1055.50 $Å^3$ in β-lactoglobulin-PFOA complex, and 585.88 $Å^3$ to 895.62 $Å^3$ in β-lactoglobulin-PFOS complex with initial cavity volumes of 896.88 $Å^3$, 831.38 $Å^3$ and 895.62 $Å^{3,}$ respectively, for the three complexes (Yadav et al., 2024). The free energy landscape

analysis of the MD simulation trajectory displayed several local minima indicated by shallow troughs thus signifying the attainment of multiple partially folded conformations by the apo-β-lactoglobulin during the trajectory but the energy landscape of β-lactoglobulin-PFAS complexes showed increase in steepness of the valley signifying attainment of global minima revealing or completely folded states in complex form (Papaleo et al., 2009).

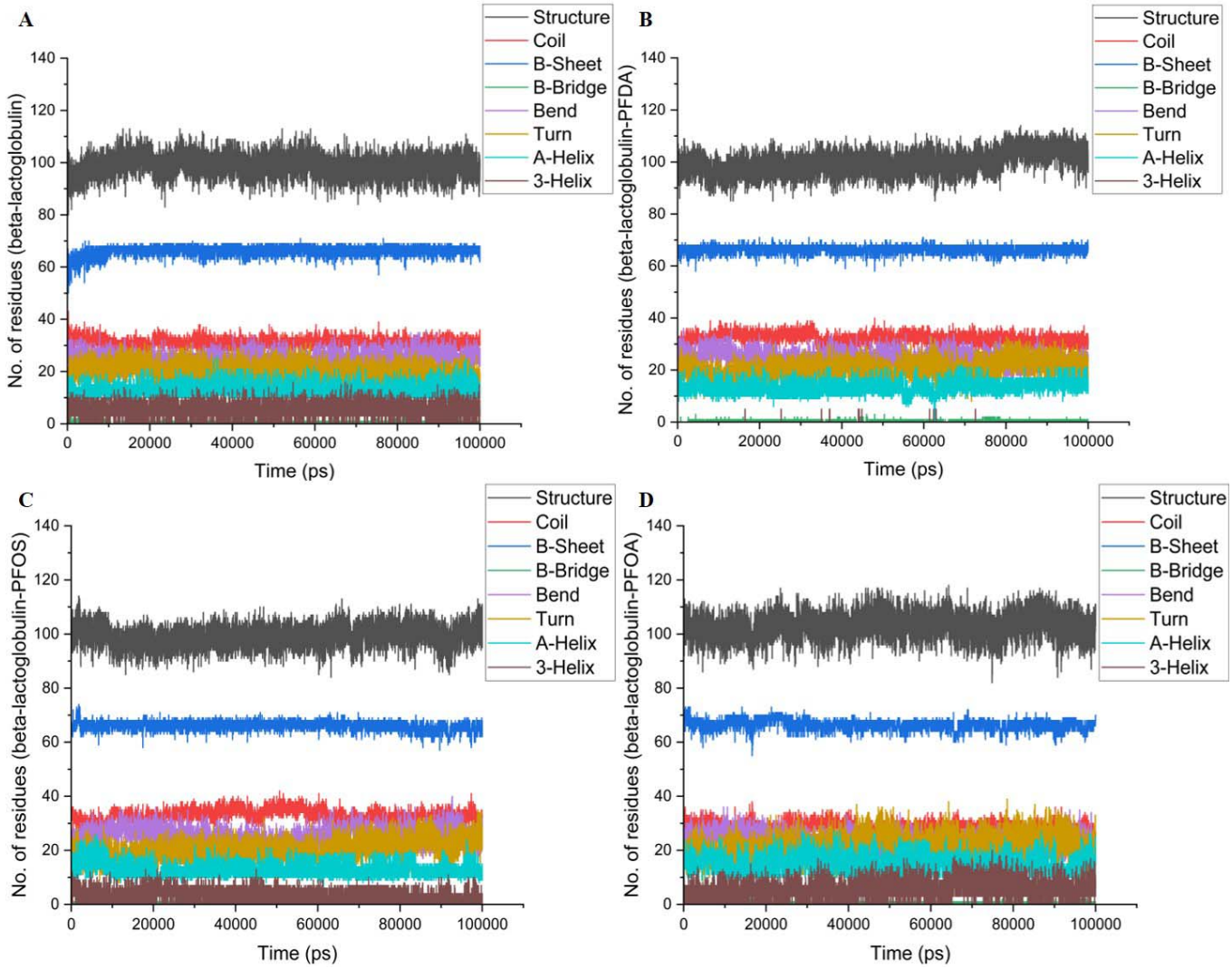

Figure 6: MD simulation trajectory analysis for variation in secondary structures in A) apo-beta-lactoglobulin, B) beta-lactoglobulin in complex with PFDA, C) beta-lactoglobulin in complex with PFOS, D) beta-lactoglobulin in complex with PFOA during the simulation trajectory of 100 ns

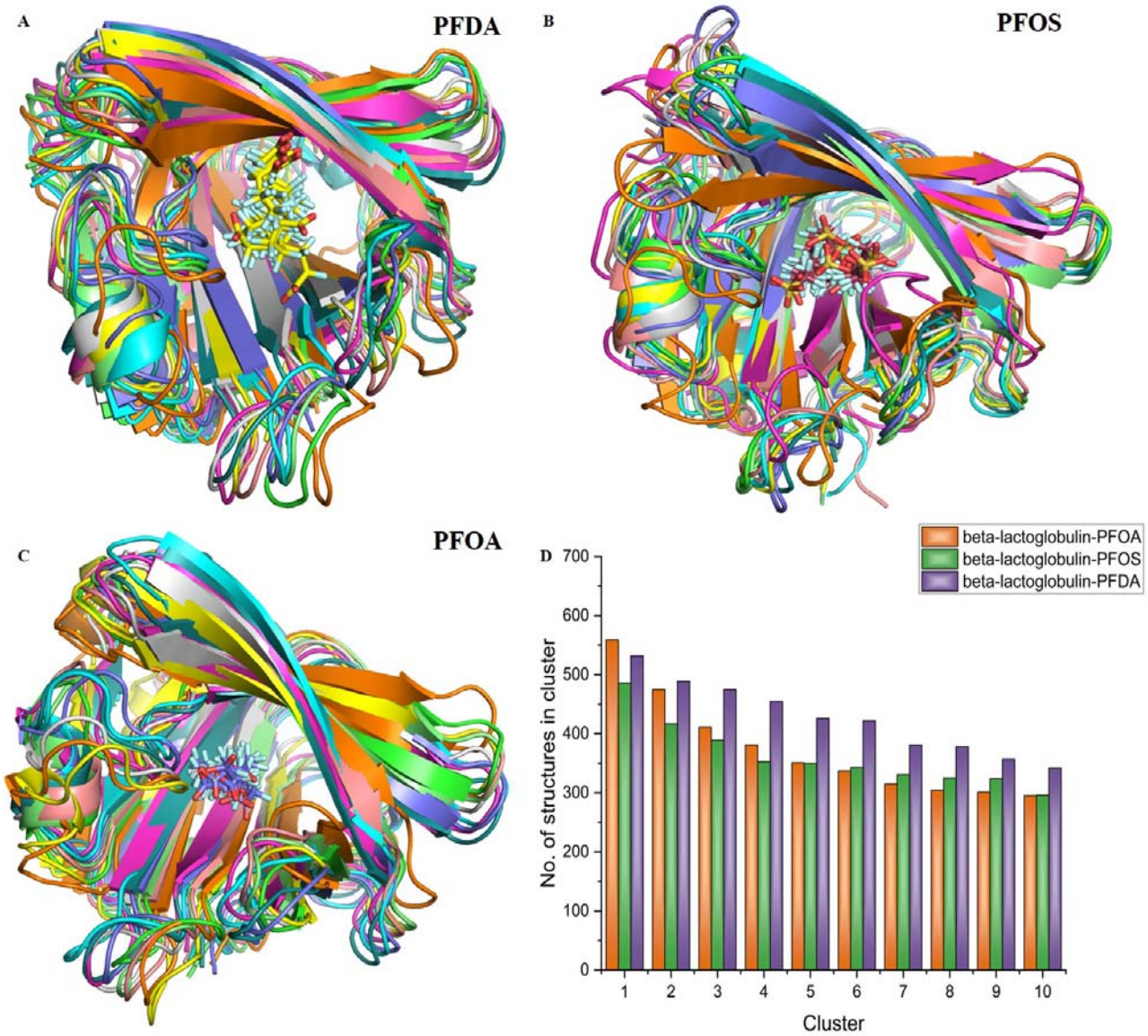

Figure 7: Clustering analysis of the MD simulation trajectories. A) Superimposition of representative conformations of the top 10 clusters analyzed from the simulation trajectory of beta-lactoglobulin-PFDA complex B) Superimposition of representative conformations of the top 10 clusters analyzed from the simulation trajectory of beta-lactoglobulin-PFOS complex C) Superimposition of representative conformations of the top 10 clusters analyzed from the simulation trajectory of beta-lactoglobulin-PFOA complex D) Bar plot showing number of structures identified in top 10 cluster from the simulation trajectories of beta-lactoglobulin-PFASs complexes.

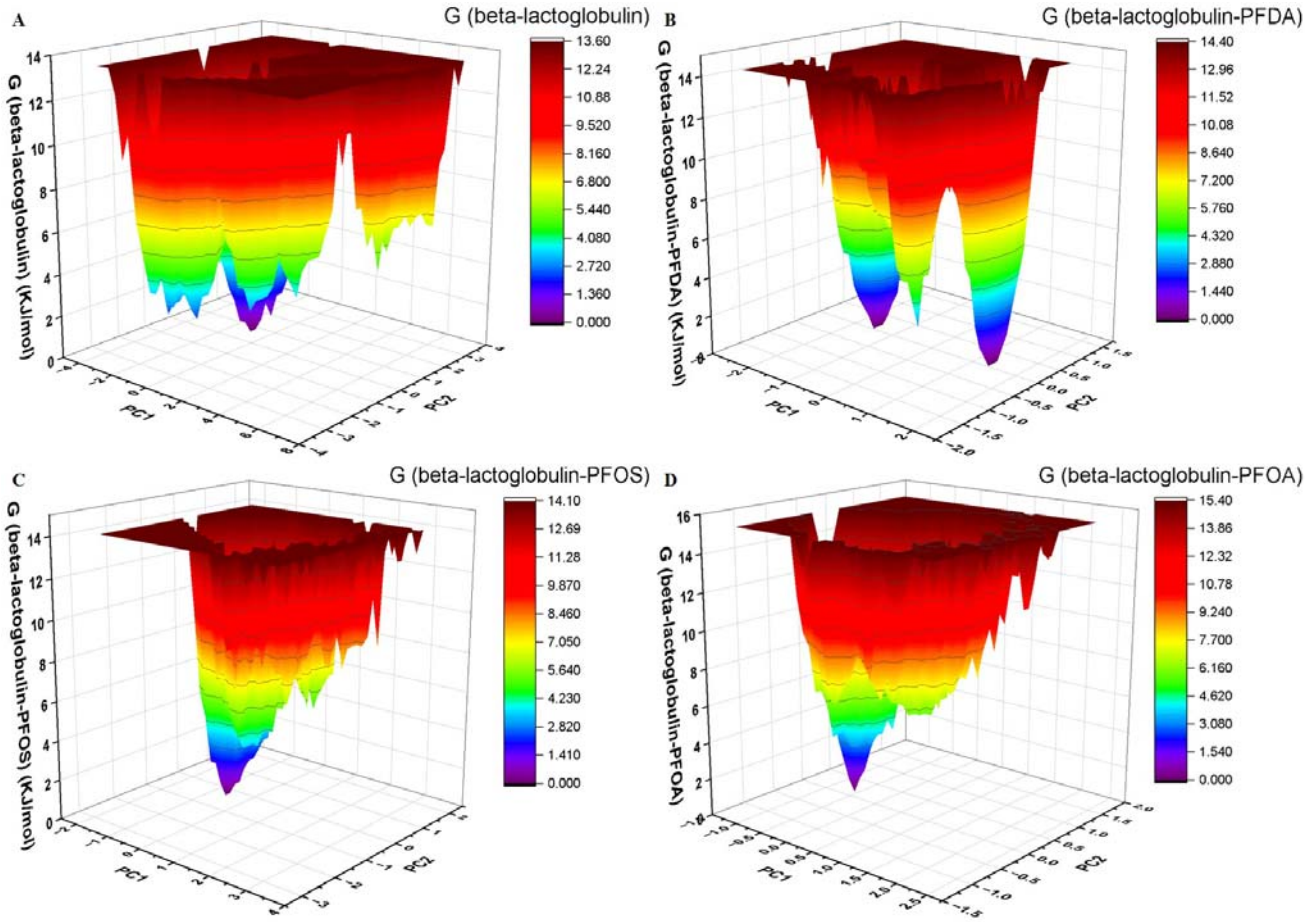

Figure 8: Gibbs Free energy landscapes of A) apo-beta-lactoglobulin B) beta-lactoglobulin-PFDA complex C) beta-lactoglobulin-PFOS complex D) beta-lactoglobulin-PFOA complex, showing an increase in thermodynamic stability of beta-lactoglobulin in complex forms.

End state free energy analysis of the β-lactoglobulin-PFDA, β-lactoglobulin-PFOS, and β-lactoglobulin-PFOA complexes during the last 40 ns of the simulation trajectories was analyzed. Different energy components, including van der Waals, electrostatic interaction energy, polar bond energy, and non-polar bond energy, resulted in a high negative total binding energy, indicating consistent effective binding of the PFAS compounds in the central calyx of the β-lactoglobulin. The average total binding energies of PFDA, PFOS, and PFOA in the β-lactoglobulin calyx were -25.04, -21.47, and -22.89 kcal/mol, respectively. Out of all evaluated energy components, the hydrophobic van der Waals interactions energy component was the leading contributor to the total binding energy, accounting for -32.04, -27.63, and -31.62 kcal/mol, respectively, for β-lactoglobulin PFDA, PFOS, and PFOA complexes,

therefore confirming effective PFAS binding in β-lactoglobulin (Valdés-Tresanco et al., 2021).

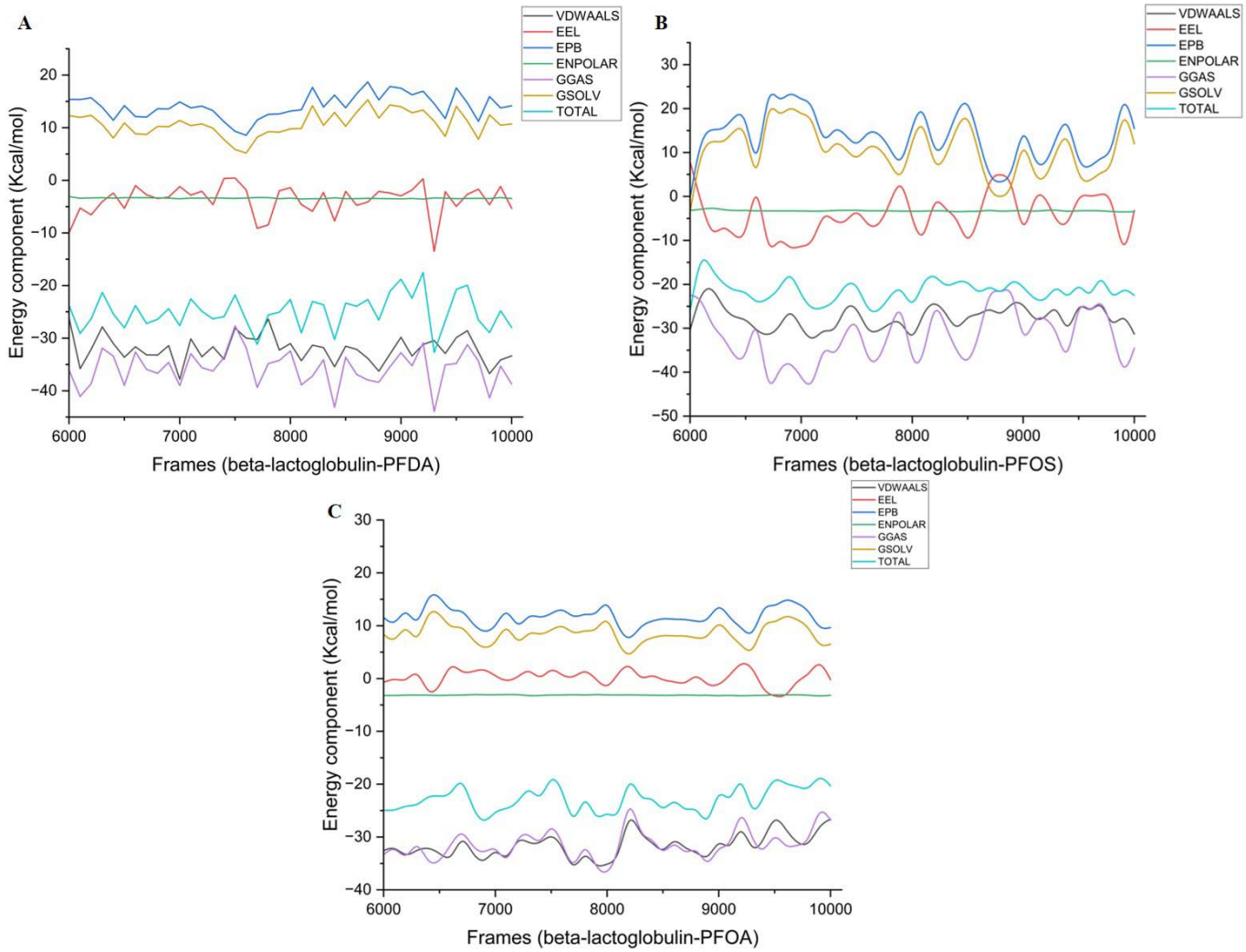

Figure 9: End state free binding energy analysis of beta-lactoglobulin in complex with A). PFDA, B) PFOS, C) PFOA showing variation in different energy components during the last 40 ns of the simulation trajectory. (VDWAALS: van der Waals, EEL: Electrostatic interaction energy, EPB: Polar bond energy, ENPOLAR: Non-polar bond energy, GGAS: VDWAALS + EEL, GSOLV: ENPOLAR + EPB, TOTAL = GGAS + GSOLV)

However, several hypotheses associated with β-lactoglobulin PFAS binding have been assumed; the present study provides the exact binding mechanism of PFAS within the central calyx cavity of the β-lactoglobulin by determining the crystal structures of β-lactoglobulin-PFDA, β-lactoglobulin-PFOS, and β-lactoglobulin-PFOA complexes and further analyzing their binding dynamics using an in-silico approach. The findings illustrated in the present

analysis provide valuable insights associated with PFAS transport to neonates via mother's milk or infant formulations, resulting in increased toxicity, and can be beneficial in developing strategies to reduce toxicity by inhibiting PFAS binding in the central calyx of the β-lactoglobulin.

Conclusion

This structural study identifies with atomic- and molecular-precision the interactions between three widely-prevalent PFAS molecules and β-lactoglobulin. It helps begin to reduce knowledge gaps in the first and subsequent molecular events that potentially onset PFAS-associated perturbations in β-lactoglobulin proteins, which drive specific toxicological effects in humans. It can form the foundation for cataloguing energetics, sterics, and intermolecular-interactions-based descriptors that are dependent upon PFAS head-group, chain length, and hydrophobicity as a function of protein side-chain and topology.

Statements and Declarations

Funding and Facilities

"This work was supported by a DBT-funded projects entitled Translational and Structural Bioinformatics – BIC at the Department of Biotechnology, Indian Institute of Technology, Roorkee (BT/PR40141/BTIS/137/16/2021) and National Network Project of Department of Biotechnology, Indian Institute of Technology, Roorkee (BT/PR40142/BTIS/137/72/2023).

Competing Interests

"The authors have no relevant financial or non-financial interests to disclose."

Authors Contributions

"The study conception and design were carried out by Pravindra Kumar and Mahesh Narayan. Crystallization experiments and data collection were performed by Shalja Verma and Anika Singh. In-silico analysis was performed by Shalja Verma, Anika Singh, and Lela Vukovic. The first draft of the manuscript was written by Shalja Verma, Pravindra Kumar, and Mahesh Narayan. All authors commented on previous versions of the manuscript and read and approved the final manuscript."

Ethics approval

Not applicable

Declaration of generative AI

AI-based tool has not been used for this manuscript

References

1. O'Hagan, D. (2007). Understanding organofluorine chemistry. An introduction to the C–F bond. Chemical Society Reviews, 37(2), 308–319. https://doi.org/10.1039/b711844a
2. Kraka, E., & Cremer, D. (2009). Characterization of CF Bonds with Multiple□Bond Character: Bond Lengths, Stretching Force Constants, and Bond Dissociation Energies. ChemPhysChem, 10(4), 686–698. https://doi.org/10.1002/cphc.200800699
3. Marshall, P., & Schwartz, M. (1997). Computational study of C−H bond strengths in polyfluoroalkanes. The Journal of Physical Chemistry A, 101(15), 2906–2909. https://doi.org/10.1021/jp963992x
4. Key, B. D., Howell, R. D., & Criddle, C. S. (1997). Fluorinated organics in the biosphere. Environmental Science & Technology, 31(9), 2445–2454. https://doi.org/10.1021/es961007c
5. DeLuca, N. M., Minucci, J. M., Mullikin, A., Slover, R., & Hubal, E. a. C. (2022). Human exposure pathways to poly- and perfluoroalkyl substances (PFAS) from indoor media: A systematic review. Environment International, 162, 107149. https://doi.org/10.1016/j.envint.2022.107149
6. Panieri, E., Baralic, K., Djukic-Cosic, D., Djordjevic, A. B., & Saso, L. (2022). PFAS molecules: a major concern for the human health and the environment. Toxics, 10(2), 44. https://doi.org/10.3390/toxics10020044
7. Fenton, S. E., Ducatman, A., Boobis, A., DeWitt, J. C., Lau, C., Ng, C., Smith, J. S., & Roberts, S. M. (2020). Per□ and Polyfluoroalkyl Substance Toxicity and Human Health Review: Current State of Knowledge and Strategies for Informing Future Research. Environmental Toxicology and Chemistry, 40(3), 606–630. https://doi.org/10.1002/etc.4890
8. Boyd, R. I., Ahmad, S., Singh, R., Fazal, Z., Prins, G. S., Erdogan, Z. M., Irudayaraj, J., & Spinella, M. J. (2022). Toward a mechanistic understanding of poly- and perfluoroalkylated substances and cancer. Cancers, 14(12), 2919. https://doi.org/10.3390/cancers14122919
9. Bharal, B., Ruchitha, C., Kumar, P., Pandey, R., Rachamalla, M., Niyogi, S., Naidu, R., & Kaundal, R. K. (2024). Neurotoxicity of per- and polyfluoroalkyl substances:

Evidence and future directions. The Science of the Total Environment, 176941. https://doi.org/10.1016/j.scitotenv.2024.176941

10. Starnes, H. M., Rock, K. D., Jackson, T. W., & Belcher, S. M. (2022). A Critical Review and Meta-Analysis of Impacts of Per- and Polyfluorinated Substances on the Brain and Behavior. Frontiers in Toxicology, 4. https://doi.org/10.3389/ftox.2022.881584
11. Roy, V. C., Bala, R., & Mehta, S. (2025). Poly- and per-fluoroalkyl substances toxicity on skeletal and cognitive well-being: a comprehensive review. Journal of Environmental Science and Health Part C, 1–25. https://doi.org/10.1080/26896583.2025.2460884
12. Mahfouz, M., Harmouche-Karaki, M., Matta, J., Mahfouz, Y., Salameh, P., Younes, H., Helou, K., Finan, R., Abi-Tayeh, G., Meslimani, M., Moussa, G., Chahrour, N., Osseiran, C., Skaiki, F., & Narbonne, J. (2023). Maternal Serum, Cord and Human Milk Levels of Per- and Polyfluoroalkyl Substances (PFAS), Association with Predictors and Effect on Newborn Anthropometry. Toxics, 11(5), 455. https://doi.org/10.3390/toxics11050455
13. Yao, J., Dong, Z., Jiang, L., Pan, Y., Zhao, M., Bai, X., & Dai, J. (2023). Emerging and legacy Perfluoroalkyl substances in breastfed Chinese infants: renal clearance, body burden, and implications. Environmental Health Perspectives, 131(3). https://doi.org/10.1289/ehp11403
14. Nyberg, E., Awad, R., Bignert, A., Ek, C., Sallsten, G., & Benskin, J. P. (2018). Inter-individual, inter-city, and temporal trends of per- and polyfluoroalkyl substances in human milk from Swedish mothers between 1972 and 2016. Environmental Science Processes & Impacts, 20(8), 1136–1147. https://doi.org/10.1039/c8em00174j
15. Zheng, G., Schreder, E., Dempsey, J. C., Uding, N., Chu, V., Andres, G., Sathyanarayana, S., & Salamova, A. (2021). Per- and Polyfluoroalkyl Substances (PFAS) in breast milk: Concerning Trends for Current-Use PFAS. Environmental Science & Technology, 55(11), 7510–7520. https://doi.org/10.1021/acs.est.0c06978
16. Mokhtari, P., Schmidt, K. A., Babaei, M., & Goran, M. I. (2024). Altered nutrient composition of Lactose-Reduced Infant Formula. Nutrients, 16(2), 276. https://doi.org/10.3390/nu16020276
17. Martin, C., Ling, P., & Blackburn, G. (2016). Review of infant feeding: Key features of breast milk and infant formula. Nutrients, 8(5), 279. https://doi.org/10.3390/nu8050279

18. Narayan, M., & Berliner, L. J. (1997). Fatty acids and retinoids bind independently and simultaneously to B-Lactoglobulin. Biochemistry, 36(7), 1906–1911. https://doi.org/10.1021/bi9621526
19. Tai, C. S., Chen, Y. Y., & Chen, W. L. (2016). B-Lactoglobulin influences human immunity and promotes cell proliferation. BioMed Research International, 2016, 1–12. https://doi.org/10.1155/2016/7123587
20. Perez, M., Sanchez, L., Aranda, P., Ena, J., Oria, R., & Calvo, M. (1992). Effect of β-lactoglobulin on the activity of pregastric lipase. A possible role for this protein in ruminant milk. Biochimica Et Biophysica Acta (BBA) - Lipids and Lipid Metabolism, 1123(2), 151–155. https://doi.org/10.1016/0005-2760(92)90105-5
21. Schwieger, C., & Ropers, M. (2012). Binding of a perfluorinated surfactant to β-lactoglobulin in aqueous solutions. Food Hydrocolloids, 30(1), 241–248. https://doi.org/10.1016/j.foodhyd.2012.05.021
22. Pham, P. C., Taylor, M., Nguyen, G. T. H., Beltran, J., Bennett, J. L., Ho, J., & Donald, W. A. (2024). Binding of Per- and Polyfluoroalkyl Substances to β-Lactoglobulin from Bovine Milk. Chemical Research in Toxicology, 37(5), 757–770. https://doi.org/10.1021/acs.chemrestox.4c00021
23. Yadav, A., Vuković, L., & Narayan, M. (2024). An Atomic and Molecular Insight into How PFOA Reduces α-Helicity, Compromises Substrate Binding, and Creates Binding Pockets in a Model Globular Protein. Journal of the American Chemical Society, 146(18), 12766–12777.
24. Wu, S., Pérez, M. D., Puyol, P., & Sawyer, L. (1999). β-Lactoglobulin Binds Palmitate within Its Central Cavity. Journal of Biological Chemistry, 274(1), 170–174. https://doi.org/10.1074/jbc.274.1.170
25. Dessau, M. A., & Modis, Y. (2011). Protein crystallization for x-ray crystallography. Journal of Visualized Experiments, 47. https://doi.org/10.3791/2285
26. Potterton, L., Agirre, J., Ballard, C., Cowtan, K., Dodson, E., Evans, P. R., Jenkins, H. T., Keegan, R., Krissinel, E., Stevenson, K., Lebedev, A., McNicholas, S. J., Nicholls, R. A., Noble, M., Pannu, N. S., Roth, C., Sheldrick, G., Skubak, P., Turkenburg, J., . . . Wojdyr, M. (2018). CCP4i2: the new graphical user interface to theCCP4 program suite. Acta Crystallographica Section D Structural Biology, 74(2), 68–84. https://doi.org/10.1107/s2059798317016035

27. Evans, P. R., & Murshudov, G. N. (2013). How good are my data and what is the resolution? Acta Crystallographica Section D Biological Crystallography, 69(7), 1204–1214. https://doi.org/10.1107/s0907444913000061
28. Vagin, A., & Teplyakov, A. (2009). Molecular replacement with MOLREP. Acta Crystallographica Section D Biological Crystallography, 66(1), 22–25. https://doi.org/10.1107/s0907444909042589
29. Emsley, P., Lohkamp, B., Scott, W. G., & Cowtan, K. (2010). Features and development of Coot. Acta Crystallographica Section D Biological Crystallography, 66(4), 486–501. https://doi.org/10.1107/s0907444910007493
30. Murshudov, G. N., Skubák, P., Lebedev, A. A., Pannu, N. S., Steiner, R. A., Nicholls, R. A., Winn, M. D., Long, F., & Vagin, A. A. (2011). REFMAC5 for the refinement of macromolecular crystal structures. Acta Crystallographica Section D Biological Crystallography, 67(4), 355–367. https://doi.org/10.1107/s0907444911001314
31. Adams, P. D., Afonine, P. V., Bunkóczi, G., Chen, V. B., Davis, I. W., Echols, N., Headd, J. J., Hung, L., Kapral, G. J., Grosse-Kunstleve, R. W., McCoy, A. J., Moriarty, N. W., Oeffner, R., Read, R. J., Richardson, D. C., Richardson, J. S., Terwilliger, T. C., & Zwart, P. H. (2010). PHENIX: a comprehensive Python-based system for macromolecular structure solution. Acta Crystallographica Section D Biological Crystallography, 66(2), 213–221. https://doi.org/10.1107/s0907444909052925
32. Pettersen, E. F., Goddard, T. D., Huang, C. C., Meng, E. C., Couch, G. S., Croll, T. I., Morris, J. H., & Ferrin, T. E. (2020). UCSF ChimeraX: Structure visualization for researchers, educators, and developers. Protein Science, 30(1), 70–82. https://doi.org/10.1002/pro.3943
33. Rigsby, R. E., & Parker, A. B. (2016). Using the PyMOL application to reinforce visual understanding of protein structure. Biochemistry and Molecular Biology Education, 44(5), 433–437. https://doi.org/10.1002/bmb.20966
34. Pronk, S., Páll, S., Schulz, R., Larsson, P., Bjelkmar, P., Apostolov, R., Shirts, M. R., Smith, J. C., Kasson, P. M., Van Der Spoel, D., Hess, B., & Lindahl, E. (2013). GROMACS 4.5: a high-throughput and highly parallel open source molecular simulation toolkit. Bioinformatics, 29(7), 845–854. https://doi.org/10.1093/bioinformatics/btt055
35. Vanommeslaeghe, K., Hatcher, E., Acharya, C., Kundu, S., Zhong, S., Shim, J., Darian, E., Guvench, O., Lopes, P., Vorobyov, I., & Mackerell, A. D. (2009).

CHARMM general force field: A force field for drug□like molecules compatible with the CHARMM all□atom additive biological force fields. Journal of Computational Chemistry, 31(4), 671–690. https://doi.org/10.1002/jcc.21367

36. Huang, J., & MacKerell, A. D. (2013). CHARMM36 all-atom additive protein force field: Validation based on comparison to NMR data. Journal of Computational Chemistry, 34(25), 2135–2145. https://doi.org/10.1002/jcc.23354
37. Hollingsworth, S. A., & Dror, R. O. (2018). Molecular dynamics simulation for all. Neuron, 99(6), 1129–1143. https://doi.org/10.1016/j.neuron.2018.08.011
38. 15. Papaleo, E., Mereghetti, P., Fantucci, P., Grandori, R., & De Gioia, L. (2009). Free-energy landscape, principal component analysis, and structural clustering to identify representative conformations from molecular dynamics simulations: The myoglobin case. Journal of Molecular Graphics and Modelling, 27(8), 889–899. https://doi.org/10.1016/j.jmgm.2009.01.006
39. Valdés-Tresanco, M. S., Valdés-Tresanco, M. E., Valiente, P. A., & Moreno, E. (2021). gmx_MMPBSA: A New Tool to Perform End-State Free Energy Calculations with GROMACS. Journal of Chemical Theory and Computation, 17(10), 6281–6291. https://doi.org/10.1021/acs.jctc.1c00645
40. Leung, S. C. E., Wanninayake, D., Chen, D., Nguyen, N., & Li, Q. (2023). Physicochemical properties and interactions of perfluoroalkyl substances (PFAS) - Challenges and opportunities in sensing and remediation. The Science of the Total Environment, 905, 166764. https://doi.org/10.1016/j.scitotenv.2023.166764 https://doi.org/10.1021/jacs.4c02934
41. Kontopidis, G., Holt, C., & Sawyer, L. (2002). The ligand-binding site of bovine B-Lactoglobulin: evidence for a function? Journal of Molecular Biology, 318(4), 1043–1055. https://doi.org/10.1016/s0022-2836(02)00017-7
42. Adams, J. J., Anderson, B. F., Norris, G. E., Creamer, L. K., & Jameson, G. B. (2006). Structure of bovine β-lactoglobulin (variant A) at very low ionic strength. Journal of Structural Biology, 154(3), 246–254. https://doi.org/10.1016/j.jsb.2005.12.010
43. Ormeño, F., & General, I. J. (2024). Convergence and equilibrium in molecular dynamics simulations. Communications Chemistry, 7(1). https://doi.org/10.1038/s42004-024-01114-5
44. Badar, M. S., Shamsi, S., Ahmed, J., & Alam, M. A. (2022). Molecular Dynamics Simulations: Concept, Methods, and Applications. In Integrated science (pp. 131–151). https://doi.org/10.1007/978-3-030-94651-7_7

Figure Captions

Figure 1: Superimposition of crystal structures of beta-lactoglobulin in complex with PFOS (ruby), PFOA (blue), PFDA (yellow) A). Vertical view showing 9 beta-strands interspersed by loops and helices forming a central calyx with all three compounds bound into it. B) Horizontal view showing the same binding site inside the central calyx for all three compounds. C) Hydrophobic surface view of beta-lactoglobulin showing the presence of highly hydrophobic residues inside the central calyx. (Hydrophobic residue: white, hydrophilic residues: blue)

Figure 2: Crystal structures of beta-lactoglobulin with PFASs. A) Electron density Fo-Fc map contoured at 3σ of Perfluorooctane sulfonic acid (PFOS) in complex with beta-lactoglobulin at 2.5 Å B) Stick representation of interacting residues (orange) with PFOS (ruby) in the central calyx of beta-lactoglobulin. C) Electron density Fo-Fc map contoured at 3σ of Perfluorooctanoic acid (PFOA) in complex with beta-lactoglobulin at 2.0Å D) Stick representation of interacting residues (orange) with PFOA (blue) in the central calyx of beta-lactoglobulin E) Electron density Fo-Fc map contoured at 3σ of Perfluorodecanoic acid (PFDA) in complex with beta-lactoglobulin at 2.0 Å F) Stick representation of interacting residues (orange) with PFDA (yellow) in the central calyx of beta-lactoglobulin

Figure 3: Comparative structural analysis of closed and open conformations of the β-lactoglobulin-PFAS complexes. A) Cartoon representation of superimposed structures of apo-β-lactoglobulin closed (blue) conformation (PDB ID: 2AKQ, previous study) over open conformation (green) of β-lactoglobulin-PFAS complexes (present study), representing structural changes highlighted in dark green colour for open conformation and dark blue colour for closed conformation. B) Surface view of the apo-β-lactoglobulin closed (blue) conformation (PDB ID: 2AKQ, previous study) C) Surface view of open conformation (green) of β-lactoglobulin-PFAS complexes D) Superimposed surface view of closed (blue) and open (green) conformations of β-lactoglobulin.

Figure 4: MD simulation analysis of apo-beta-lactoglobulin and crystal structures of beta-lactoglobulin in complex with PFOA, PFOS, and PFDA. A) Root Mean Square Deviation

(RMSD) versus time plots B) Radius of gyration (Rg) versus time plots C) Root Mean Square Fluctuations (RMSF) versus residue plots D) B-Factor versus residue plots during 100 ns of simulation trajectory E) Solvent Accessible Surface Area (SASA) versus time plots F) Number of Hydrogen bonds versus time plots.

Figure 5: Superimposition of extracted frames at every 10 ns of the MD simulation trajectories of apo-beta-lactoglobulin and crystal structures of beta-lactoglobulin in complex with PFOA, PFOS, and PFDA. The region showing major changes in the B-factor has been marked. Structures in green colour show the initial conformations at 0 ns

Figure 6: MD simulation trajectory analysis for variation in secondary structures in A) apo-beta-lactoglobulin, B) beta-lactoglobulin in complex with PFDA, C) beta-lactoglobulin in complex with PFOS, D) beta-lactoglobulin in complex with PFOA during the simulation trajectory of 100 ns

Figure 7: Clustering analysis of the MD simulation trajectories. A) Superimposition of representative conformations of the top 10 clusters analyzed from the simulation trajectory of beta-lactoglobulin-PFDA complex B) Superimposition of representative conformations of the top 10 clusters analyzed from the simulation trajectory of beta-lactoglobulin-PFOS complex C) Superimposition of representative conformations of the top 10 clusters analyzed from the simulation trajectory of beta-lactoglobulin-PFOA complex D) Bar plot showing number of structures identified in top 10 cluster from the simulation trajectories of beta-lactoglobulin-PFASs complexes.

Figure 8: Gibbs Free energy landscapes of A) apo-beta-lactoglobulin B) beta-lactoglobulin-PFDA complex C) beta-lactoglobulin-PFOS complex D) beta-lactoglobulin-PFOA complex, showing an increase in thermodynamic stability of beta-lactoglobulin in complex forms.

Figure 9: End state free binding energy analysis of beta-lactoglobulin in complex with A). PFDA, B) PFOS, C) PFOA showing variation in different energy components during the last 40 ns of the simulation trajectory. (VDWAALS: van der Waals, EEL: Electrostatic interaction energy, EPB: Polar bond energy, ENPOLAR: Non-polar bond energy, GGAS: VDWAALS + EEL, GSOLV: ENPOLAR + EPB, TOTAL = GGAS + GSOLV)